SLAC-PUB-957
(TH)
September 1971

AN s-WAVE $I = 0$ $\pi\pi$ RESONANCE*

Bryan F. Gore

Center for Theoretical Physics
Department of Physics and Astronomy
University of Maryland
College Park, Maryland 20742

and

Central Washington State College†
Ellensburg, Washington 98926

and

Stanford Linear Accelerator Center
Stanford University
Stanford, California 94305

* Supported in part by the National Science Foundation under Grants NSF-5461 and GY-8541 and the U. S. Atomic Energy Commission. Computer time was furnished by the University of Maryland Computer Science Center under NASA Grant NsG-398. The author was a visitor at SLAC during revision of the manuscript.

† Permanent address.

(Submitted to Phys. Rev.)

ABSTRACT

Solutions are presented for subtracted dispersion relations, written for the s and p-wave inverse $\pi\pi$ scattering amplitudes with poles inserted into both s-waves. These solutions predict the existence of a broad I = 0 s-wave resonance (σ) accompanied by a small, negative I = 2 phase shift, in the absence of any s-wave experimental input. While p-wave subtraction parameters are adjusted to fit a 755 MeV ρ resonance with width 120 MeV, the s-wave parameters are determined by crossing symmetry through derivative conditions to third order. The coupling constant, λ, is a free parameter, and resonant solutions are obtained for $-.033 \leq \lambda \leq .040$ with σ masses ranging from 550 to 900 MeV. In no case does δ_0^0 rise to 135^0 by 1 BeV. Both s-wave amplitudes exhibit zeros between the cuts for $-.01 < \lambda < .02$, and for $\lambda = -.008$ the zeros coincide with those predicted by the Adler condition applied on the mass shell. Solutions with $\lambda \lesssim -.01$ satisfy crossing conditions for $\pi^0\pi^0$ amplitudes. The failure of the other solutions to satisfy them may be related to approximations made in applying crossing symmetry. A method of improving the solutions is suggested.

I. INTRODUCTION

In this paper calculations of subtracted dispersion relations written for the s and p-wave inverse $\pi\pi$ scattering amplitudes are presented. Elastic unitarity is used in the evaluation of right cut integrals, and approximate crossing symmetry in the evaluation of left cut integrals. s-wave parameters are evaluated using derivative conditions from approximate crossing symmetry, and the two p-wave subtraction constants are fixed by requiring a p-wave resonance of mass 755 MeV and width 120 MeV, the ρ. The Chew-Mandelstam coupling constant, λ, is treated as a free parameter, and orders the solutions.

Pole terms are inserted into the s-wave inverse amplitudes, and allow the possibility of zeros in both s-wave partial wave amplitudes. While such zeros have been predicted from PCAC considerations,[1] no conditions from current algebra are imposed in these calculations. In fact, since crossing symmetry requires the first derivatives of the s-wave inverse amplitudes to be proportional to λ^{-2}, it is clear that for small $|\lambda|$ this condition cannot be satisfied by dispersion integrals unless further structure is built in. Thus the motivation for the introduction of the pole terms into the inverse amplitudes is contained within this formalism. Nevertheless, for solutions obtained the positions of the zeros of the I = 0 and 2 s-wave amplitudes, plotted one against the other, lie on a straight line passing through the point predicted by PCAC.

Solutions are presented for the range $-.03 < \lambda < .10$. Within the range $-.03 < \lambda < .04$ these solutions exhibit an I = 0 s-wave resonance, the σ, with mass increasing from 550 MeV for $\lambda = -.033$ to 900 MeV for $\lambda = .04$. The expected weakening of the interaction with increasing λ is seen in the behavior of the resonance mass, and in a transition solution (δ_0^0 small and negative below 700 MeV, small and positive above) for $\lambda = .100$ linking the resonant solutions

to repulsive s-wave dominant solutions previously reported for large positive λ.[2-4] While solutions could not be obtained for $\lambda < -.033$, projecting an increasing attraction with decreasing λ indicates the probable establishment of a bound state for larger negative λ which has already been reported in results which failed to exhibit resonant behavior.[3,4] Thus, these solutions provide an understanding of the interaction as a function of λ which explains earlier results whose interpretation was previously unclear.

A series of calculations leading to the results noted above is presented here. With λ fixed a priori, five conditions are necessary to evaluate the six s-wave parameters introduced by subtractions and pole terms. To second derivatives in the s-waves, approximate crossing symmetry yields four conditions, and a single third derivative condition has been previously derived by the author[5] (Ref. 5 will henceforth be referred to as I). Since the third derivative condition is difficult to apply to the inverse amplitudes, initially it was not used to evaluate parameters in the calculations reported here. Instead, first, a σ resonance of mass 745 MeV was required. In the solutions thus obtained, the s-wave I = 2 phase shift at the mass of the ρ resonance varied (as a function of λ) over the range $-43^{\circ} \leq \delta_0^2 \leq -13^{\circ}$. The third derivative equation was satisfied by a solution with $\delta_0^2 = -19^{\circ}$.

Next, the σ condition was removed and the value of δ_0^2 at the ρ mass was fixed. Solutions were obtained for δ_0^2 values of -20°, -15° and -10°. In those solutions exhibiting an I = 0 s-wave resonance, the mass of the σ was found to depend on both the value of λ and the value at which δ_0^2 was fixed. However, for each choice of δ_0^2, the third derivative condition was satisfied by only one solution. Examination of the three solutions satisfying this condition revealed the already described correlation of resonance mass with λ.

This demonstration that the imposition of the third derivative crossing condition allowed the selection of solutions with I = 0 s-waves having a sensible dependence on λ (including one in excellent agreement with experiment), provided sufficient motivation to impose it in place of any condition from experiment. When this was done the iterations converged, yielding the resonant solutions varying appropriately with λ which have already been described.

II. FORMALISM

In terms of the variable $\nu = s/4 - 1$, where s is the center of mass energy squared (natural units, $m_\pi = 1$), the unitarity condition for elastic scattering is

$$A_\ell^I(\nu) = [(\nu+1)/\nu]^{1/2}\left(\cot \delta_\ell^I - i\right)^{-1} , \tag{1}$$

where $\nu > 0$ and the phase shifts, δ_ℓ^I, are real. This relation is assumed valid within the energy range of these calculations. The once subtracted dispersion relations for the s-wave inverse amplitudes $F_I(\nu) = A_0^I(\nu)^{-1}$, with pole terms inserted, are

$$F_{I=0,2}(\nu) = \alpha_I + \beta_I/(1-\gamma_I\nu) + f(\nu) + L_I(\nu) - i\mathcal{I}_I(\nu) \tag{2}$$

and the twice subtracted p-wave dispersion relation, written for $F_1(\nu) = \nu A_1^1(\nu)^{-1}$ is

$$F_1(\nu) = \alpha_1 + \beta_1\nu + \nu f(\nu) + L_1(\nu) - i\nu\mathcal{I}_1(\nu) . \tag{3}$$

($F_1(\nu)$ lacks the threshold pole of $A_1^1(\nu)^{-1}$.) The integral over the right hand cut discontinuity (given by unitarity) is

$$f(\nu) = -\frac{\nu}{\pi} P\int_0^\infty \frac{[\nu'/(\nu'+1)]^{1/2}}{\nu'(\nu'-\nu)}\, d\nu'$$

$$= \frac{2}{\pi}\left(\frac{\nu}{\nu+1}\right)^{1/2} \ell n\left(\sqrt{|\nu+1|} + \sqrt{|\nu|}\right)$$

$$\text{for } \nu > 0 \text{ or } \nu < -1$$

$$= \frac{2}{\pi}\left(\frac{-\nu}{1+\nu}\right)^{1/2} \tan^{-1}\left(\frac{1+\nu}{-\nu}\right)^{1/2}$$

$$\text{for } -1 < \nu < 0 . \tag{4}$$

The integral over the left hand cut discontinuity is

$$L_I(\nu) = -\frac{\nu^{\ell+1}}{\pi} P\int_{-\infty}^{-1} \frac{\text{Im } A_\ell^I(\nu')d\nu'}{\nu'(\nu'-\nu)\,|A_\ell^I(\nu')|^2} , \tag{5}$$

and the imaginary parts of the inverse amplitudes are

$$\mathcal{I}_I(\nu) = \left(\frac{\nu}{\nu+1}\right)^{1/2} \theta(\nu) + \frac{\text{Im } A_\ell^I(\nu)}{|A_\ell^I(\nu)|} \theta(-\nu-1) \quad . \tag{6}$$

Using approximate crossing symmetry, the left hand cut discontinuity is expressed in terms of the right hand cut discontinuity in the crossed channels;

$$\text{Im } A_\ell^I(\nu) = \frac{2}{\nu}\int_0^{-\nu-1} d\nu' \; P_\ell \left(1 + 2\frac{\nu'+1}{\nu}\right)$$
$$\times \sum_{I'} \chi_{II'} \sum_{\ell'} (2\ell'+1) P_{\ell'}\left(1 + 2\frac{\nu+1}{\nu'}\right) \text{Im } A_{\ell'}^{I'}(\nu') \tag{7}$$

where χ is the usual crossing matrix

$$\chi = \begin{pmatrix} 1/3 & 1 & 5/3 \\ 1/3 & 1/2 & -5/6 \\ 1/3 & -1/2 & 1/6 \end{pmatrix} \tag{8}$$

and the partial wave expansion is truncated after p-waves. On the right hand cut $\text{Im } A_\ell^I(\nu)$ may be written using the unitarity condition as soon as $\text{Re}\left[A_\ell^I(\nu)^{-1}\right]$ is known. Hence iteration proceeds by neglecting $L_I(\nu)$ and evaluating parameters, then computing $L_I(\nu)$, recomputing parameters, etc., until all parameters change by less than one per cent in the last iterative loop.

The eight parameters introduced by pole terms and subtractions are evaluated by a combination of conditions from crossing symmetry and experiment. The p-wave subtraction constants are fixed by the mass and width of the ρ resonance by requiring

$$\left(\frac{\nu^3}{\nu+1}\right)^{1/2} \cot \delta_1^1 \Big|_{\nu_\rho} = 0 \tag{9}$$

and

$$\frac{d}{d\nu}\left(\frac{\nu^3}{\nu+1}\right)^{1/2} \cot\delta\,{}^{1}_{1}\Big|_{\nu_\rho} = -\frac{1}{\gamma}\left(\frac{\nu_\rho^3}{\nu_\rho+1}\right)^{1/2} \tag{10}$$

with $\nu_\rho = 6.25$ and $\gamma = 1.15$, corresponding to a resonance of mass 755 MeV and width 120 MeV. Thus, at the ρ resonance the p wave has the same slope as if it were given by the Breit-Wigner form

$$A^{1}_{1}(\nu) = \left(\frac{\nu+1}{\nu}\right)^{1/2} \frac{\gamma}{\nu_\rho - \nu - i\gamma} \,. \tag{11}$$

Crossing symmetry, applied at the symmetry point of the Mandelstam triangle, provides derivative conditions which may be used to evaluate parameters. Although an infinite number of conditions are available, higher partial waves become more important in higher derivative conditions. (This is because the argument of the Legendre polynomials used in the partial wave expansion contains the variable ν; the point is more completely discussed in I.) Under the assumption that d and higher partial waves are small at the symmetry point, they may be neglected in the zeroth and first derivative equations with little effect. The resulting approximate crossing conditions, to be avaluated at the symmetry point $\nu_{sp} = -\frac{2}{3}$ are:

$$2A^{0}_{0} = 5A^{2}_{0} \tag{12}$$

$$\frac{dA^{0}_{0}}{d\nu} = -9A^{1}_{1} \,, \tag{13}$$

$$\frac{dA^{2}_{0}}{d\nu} = \frac{9}{2}A^{1}_{1} \tag{14}$$

To derive a second derivative condition of corresponding accuracy, Chew and Mandelstam[6] reduced the d-wave effects by approximating each d-wave by a one parameter fit at threshold. They then combined the three independent second derivative equations to eliminate the d-waves, obtaining the following approximate crossing condition for application at the symmetry point

$$\frac{d^2A_0^0}{d\nu^2} - \frac{5}{2}\frac{d^2A_0^2}{d\nu^2} = 27A_1^1 + 18\frac{dA_1^1}{d\nu} . \tag{15}$$

Proceeding in this spirit, in I a single approximate third derivative equation was derived by approximating each d-wave by a two parameter threshold fit, the f-wave by a one parameter threshold fit, and removing the five parameters by combining equations. This approximate crossing condition, to be evaluated at the symmetry point, is

$$-\frac{1}{3}\left(\frac{d^3A_0^0}{d\nu^3} - \frac{5}{2}\frac{d^3A_0^2}{d\nu^3}\right) = \frac{675}{8}A_1^1 + \frac{225}{4}\frac{dA_1^1}{d\nu} + \frac{75}{4}\frac{d^2A_1^1}{d\nu^2} . \tag{16}$$

Further details and discussion are to be found in I. Due to the attention devoted to removing the effects of higher partial waves from higher derivative conditions, it is assumed that the errors incurred in applying Eqs. (15) and (16) are no greater than those in Eqs. (12) thru (14), so that their detailed application is indeed meaningful. An a posteriori discussion of errors is to be found in Section IV of this paper.

Before discussing the application of these conditions it is perhaps in order to comment upon their usefulness. In Ref. 7, Tryon comments that when d-waves are kept, the solutions of partial wave dispersion relations satisfy second and all higher derivative conditions identically; thus they are not useful to him in

determining parameters. Within the formalism used here, unless the pole term parameters are chosen to satisfy a given condition there is clearly no reason to expect it to be satisfied. Thus, for instance, the solutions here reported which were obtained without enforcing the third derivative condition failed, in general to satisfy it. Since the second and third derivative conditions enable the determination of parameters necessary for calculation they are useful within this formalism.

Although it may not be immediately obvious, the application of the derivative equations to determine parameters is straightforward. First the conditions are expressed in terms of the inverse functions F_I. With λ specified a priori, the zeroth and first order equations provide four conditions, each linear in only one of the s-wave functions $F_{0,2}$ (recall that the p-wave is completely known from the ρ mass and width):

$$\lambda = -(5F_0)^{-1} \tag{17}$$

$$= -(2F_2)^{-1} \tag{18}$$

$$\frac{dF_0}{d\nu} = -6\left(25\lambda^2 F_1\right)^{-1} \tag{19}$$

$$\frac{dF_2}{d\nu} = 3\left(4\lambda^2 F_1\right)^{-1} \tag{20}$$

While differentiation of the numerically evaluated left cut integrals is difficult after integration, Eq. (5) may be differentiated any number of time prior to the integration. Since the resulting integrals converge even more rapidly, no accuracy is lost by this procedure.

The second and third derivative conditions are slightly more complicated to apply because they involve both s-waves. Nevertheless, when a condition

from experiment is applied to either one of the s-waves, that condition plus two of the conditions (Eq. (17) - (20)) allow the evaluation of the three parameters of that partial wave via linear equations. With one s-wave known, the second derivative condition (incorporating Eqs. (17) - (20)),

$$\frac{d^2F_0}{d\nu^2} - \frac{2}{5}\frac{d^2F_2}{d\nu^2} = -(5\lambda F_1)^{-2}\left(12\frac{dF_1}{d\nu} - \frac{81}{10\lambda}\right) , \tag{21}$$

may be linearly combined with the other two equations above, specifying all parameters unambiguously. The third derivative equation (expressed incorporating Eqs. (17) - (20)),

$$\frac{d^3F_0}{d\nu^3} - \frac{2}{5}\frac{d^3F_2}{d\nu^3} - \frac{18}{5\lambda F_1}\left(2\frac{d^2F_0}{d\nu^2} + \frac{d^2F_2}{d\nu^2}\right) - \frac{7F_1^{-3}}{12}\left(\frac{9}{5\lambda}\right)^4$$

$$= 3(\lambda F_1)^{-2}\left[\left(\frac{1}{2}\frac{d^2F_1}{d\nu^2}\right) - \frac{1}{F_1}\left(\frac{dF_1}{d\nu}\right)^2\right] \tag{22}$$

may then be evaluated straightforwardly.

When Eq. (22) is used in solving for parameters, a quadratic equation results for the ratio γ_I/β_I for one of the s-waves. Consequently, two sets of parameters are produced. In general, initially choosing the set with $\alpha_0 < 0$, then minimizing the change in γ_0 resulted in solutions, while the opposite initial choice led to imaginary roots. However, for $\lambda < -.008$ the initial roots were imaginary. This difficulty was overcome by assuming intial values for the $L_I(\nu)$

and their derivatives at the symmetry point taken from solutions obtained for the same λ values when the resonance was required. Even this technique failed for $\lambda < -.033$, when after a few iterations the roots became imaginary.

III. RESULTS

Calculations were carried out for three cases. In the first, δ_0^0 was required to resonate at 745 MeV; in the second, δ_0^2 was fixed within its experimentally determined range near the ρ mass; in the third case the third derivative condition was imposed. In all cases λ was fixed a priori as a free parameter, and solutions were obtained over as wide a range of λ as possible. Crossing conditions through the second derivative were enforced in all cases.

A. Resonance Required

The s-wave phase shifts of typical solutions obtained when a σ of 745 MeV[8] was required are shown in Fig. 1, and the related scattering lengths in Fig. 2. For $-.05 < \lambda < .05$, the scattering lengths agree within 5% with the "Universal Curve" of Morgan and Shaw[9] for a σ of 765 MeV. Thus, the general agreement found between their phase shifts and those of Fig. 1 is expected. Since the solutions presented here cover a wider range of λ, it is to be expected that as λ increases to .100 the sign change of δ_0^0 occurs at higher energy, and that as λ decreases to $-.080$, δ_0^0 increases more rapidly near threshold, than occurred in their limiting cases. Although they published no turnover δ_0^2 solutions, it may be assumed that they obtained them, since they obtained positive I=2 scattering lengths for $\lambda < -.03$. A notable difference, however, is seen when the δ_0^0 curves of Fig. 1 are compared with those of Morgan and Shaw near the σ resonance. Their solutions, obtained by treating the width of the σ as an input parameter, exhibit a wide range of widths, while the formalism used here predicts only very broad, asymmetric resonances. This result is in agreement

with their conclusion that solutions with broad σ's are preferable.

The third derivative condition, Eq. (16), is plotted in Fig. 3. In order to display the results for a wide range of λ, the vertical scale has been compressed, minimizing the visual impact of the intersection of these curves. Nevertheless, the curves clearly intersect, predicting "best" solutions with λ values of .03 and .10. In Fig. 1, for a solution with λ=.03, the value of δ_0^2 near the ρ mass would be about -19°, in acceptable agreement with recent estimates. (The other solution is discounted since its large negative α_0 and its δ_0^0 turnover above 500 MeV are contrary to experimental indications.)

Having demonstrated that the inverse amplitude formalism used here leads to sensible solutions when the σ is put in, it is hard to avoid asking whether or not other input can lead to solutions predicting a σ. A logical way to find out is to replace the condition fixing δ_0^0 with one fixing δ_0^2. The next section documents the results of such calculations.

B. δ_0^2 Fixed Near the ρ

Figs. 4-7 show the s-wave phase shifts of typical solutions obtained when the value of δ_0^2 at 745 MeV[8] was fixed in its experimentally determined range. The reproducibility of results within this formalism may be seen as follows: from Fig. 1, a σ near the ρ mass is predicted for $\lambda \approx .04$ when $\delta_0^2 = -20^\circ$; it is seen in Fig. 4 for $\lambda = -.038$. A similar σ may be expected for $\lambda \approx 0$ when $\delta_0^2 = -15^\circ$, and is seen in Fig. 5 for $\lambda = -.002$. The incompatibility, seen in Fig. 1, of a σ near the ρ mass and $\delta_0^2 = -10^\circ$ is evident in the lack of such a solution in Fig. 6. Finally, for $\delta_0^2 = -20^\circ$ a σ near the ρ mass is predicted for $\lambda \approx -.06$ from Fig. 1. Although such a result was not obtained, a solution for λ=-.057, resonant at 1 BeV, is seen in Fig. 7. Thus the formalism is satisfactorily self-consistent.

The most obvious feature of Figs. 4-6, the decrease of the mass and width of the σ with increasing λ, turns out to be a misleading consequence of the constraint of δ_0^2. The decrease would seem to imply an attractive interaction, increasing in strength with λ. However, the solution for λ=.057 of Fig. 5 shows that instead of a bound state being formed for large λ (i.e. the resonance approaching, then going below threshold with increasing λ) the interaction becomes repulsive. (Since intermediate solutions of this type most often failed to converge upon iteration, this conclustion was first reached by noting that the scattering lengths of Fig. 8 did not exhibit the discontinuity which would have corresponded to the establishment of a bound state.) The pertinant feature of these solutions is instead, the advance with increasing λ, of the pole of F_0^0 (zero of δ_0^0) toward $\nu = \infty$ and its reappearance at large negative values of ν.

The true increase of attraction occurs with negative λ, culminating in the formation of the bound state seen in Fig. 7 for λ=-.67. However, only extremely heavy, broad σ's are produced here, with the lightest occurring at 1 BeV for λ=-.057. The close similarity of the solutions with $\lambda < -.13$ to the negative λ solutions obtained in I is probably due to the constraint of the I=2 s-wave imposed in I by the insertion of a pole term into only the I=0 s-wave.

In Fig. 8 the s-wave scattering lengths are plotted one against the other. The curves are from Morgan and Shaw, with the upper, middle and lower curves representing σ's of 900, 765 and 600 MeV respectively. The curve of Fig. 2, drawn for a σ of 745 MeV, would lie just slightly below the middle curve, as is expected. The progression of the points across the curves as the σ is established and moves toward threshold is in accordance with the ordering of the curves.

Order was introduced into this confusing welter of solutions by the third derivative condition. Eq. (16) applied to the various solutions, is shown in Fig. 9.

It clearly selects a single solution from each set computed for a given δ_0^2 value. For δ_0^2 values of -10^o, -15^o and -20^o the preferred solutions have λ values of $-.017$, $.007$ and $.038$, and exhibit σ resonances with masses of 600, 660, and 750 MeV. Thus, with increasing λ the σ moves away from threshold, indicating a weakening attraction. The connection of these selected solutions with the repulsive solutions found in I for large positive λ is seen by the onset of repulsion indicated by the emergence of the pole of $F_0^0(\nu)$ $\left(\text{zero of } \delta_0^0\right)$ above threshold in the solution for $\delta_0^2 = -20^o$ with $\lambda = .038$ (Fig. 4).

Thus, while restricting δ_0^2 allowed the prediction of σ resonances of various masses, a clear interpretation of the results required the additional imposition of the third derivative condition from approximate crossing symmetry. With its usefulness thus proven, the next logical step was to see if it could be used in the determination of parameters during iteration. The results of such calculations are presented in the next section.

C. Third Derivative Condition Imposed

The s-wave phase shifts for typical solutions obtained when all s-wave parameters were fixed by conditions from crossing symmetry are shown in Fig. 10. The attraction causing the resonant δ_0^0's clearly weakens with increasing λ, and the solution with $\lambda = .10$ indicates the transition to the repulsive solutions previously obtained for $\lambda > .1$. The scattering lengths for these solutions agree closely with those computed when the resonance was required, and are plotted in Fig. 11. Imaginary roots obtained in solving for parameters prevented solutions with $\lambda < -.033$ or $\lambda > .1$. Thus imposition of the third derivative condition frees the formalism from the need of s-wave input from experiment, and leads to solutions having a sensible dependence on λ.

The locations of the zeros of the s-wave amplitudes are plotted one against the other in Fig. 12. For the resonant solutions, they lie on a straight line passing through the point predicted from PCAC considerations, which coincides with the solution with $\lambda=-.008$. Since the resonant solutions obtained for the other cases exhibited zeros lying on this same line, it was felt that this must be due to some invariant feature of the formulation. The most obvious possibility was a combination of the lowest order crossing conditions. Parametrizing the s-waves by

$$A_0^I(\nu) = a_I + b_I\nu \quad , \tag{23}$$

and applying only Eqs. (12) to (14) yielded the prediction

$$\nu_2 = -.8\nu_0 - 1.2 \tag{24}$$

for comparison with the line of Fig. 12,

$$\nu_2 = .740\nu_0 - 1.17 \tag{25}$$

Since the calculated amplitudes are not linear, this is quite satisfactory agreement. The difference in slopes is mainly due to a systematic decrease, with increasing λ, of the second derivative of A_0^0 at the symmetry point.

In achieving the above prediction, it was seen that in addition, the scattering lengths would be related by

$$2a_0 - 5a_2 = 18/F_1^1(sp) \tag{26}$$

(still assuming linear s-waves). The Breit-Wigner ρ used to fix the p-wave

in Eqs. (9) and (10) corresponds to $F_1^1(sp) = 31.9$, so the scattering lengths would lie on the line

$$a_2 = .4a_0 - .113 \quad . \tag{27}$$

Now in the actual calculations, the p-wave differs from a B-W resonance due to the cut integrals. Examination of the solutions shows that $F_1^1(sp)$ increases with λ, and agrees with the B-W value for $\lambda \simeq 0$. For each solution it is straightforward to predict a line similar to Eq. (27) and (using the value of λ also) the point on the line expected if the s-wave amplitudes were linear. These predictions are shown in Fig. 11. From the surprising accuracy of these crude predictions it is clear that the scattering length curve is determined primarily by the lowest order crossing conditions and the p-wave at the symmetry point.

An indication of self consistency is provided by comparing $\text{Im } A_0^I$ for $\nu < 0$ as calculated from the crossing integral of Eq. (7) and from $\text{Im } F_I$. These quantities are plotted in Fig. 13 for the solution with $\lambda = -.008$, and the agreement is seen to be excellent out to $\nu = -6.5$. Beyond this point the curves diverge toward the different asymptotic behaviors discussed in Ref. 3. Examination of Fig. 12 shows that for $\lambda < -.01$ the pole of F_0 has moved onto the left cut and for $\lambda > .02$ the pole of F_2 has done likewise, causing the left cut discontinuity predicted from $\text{Im } F_0^0$ to disagree with crossing. However, within the range $-.01 < \lambda < .02$ left cut agreement is the same as that shown in Fig. 13.

The asymmetry of the δ_0^0 curves plus the fact that none of them rise above 135° by 1 BeV, makes it difficult, if not meaningless, to assign widths to the σ's indicated by the various curves. A common approximation is to quote the width of a Breit-Wigner resonance, the real part of whose inverse amplitude at the resonance position has the same slope. For the solutions with

λ=-.033, .007 and .040, above the resonance the square of such an amplitude falls to half of its maximum value at 710, 1050 and 2350 MeV. However, the corresponding point below the resonance lies below threshold for all solutions except that for λ=-.033, for which it lies at 310 MeV.

Resonance width is also often related to the position of an unphysical sheet pole of the scattering amplitude. When the variable ν of Eq. (2) is allowed to become complex, a zero of $F_I(\nu)$ indicates a pole of A_0^I. The sheet structure of A_0^I is such that continuation above the real axis is onto the nearby physical sheet, while continuation below the real axis is onto the unphysical sheet. In searching for complex zeros of $F_I(\nu)$ various fits to the functions were made on the real axis to facilitate continuation. For λ=.007 a zero corresponding to a pole of A_0^0 was found variously from ν=1.6-1.6i to ν=2.4-3.5i. No attempt was made to iterate or refine the pole position because it is clearly far from the physical sheet and narrow resonance formulae are no longer applicable. It is worth noting, however, that neither A_0^0 or A_0^2 were found to have poles on the nearby physical sheet by this procedure.

IV. DISCUSSION

It is seen that all solutions having zeros of both s-wave amplitudes between the cuts ($-.01 < \lambda < .02$) exhibit broadly resonant I=0 s-waves, with δ_0^0 in no case rising to 135^o by 1 BeV. Since Re F_0 falls from $+\infty$ between the cuts through zero at the resonance position a more rapid increase of δ_0^0 above the resonance mass is clearly possible within the present formalism. However, a further rise through 180^o as used by Bizzari[10] in fitting experimental data is precluded by the present formalism (an additional pole term would be required in F_0 to allow δ_0^0 to reach 180^o for finite ν). While the present calculations therefore yield no information on the existence of such structure in F_0 above the ρ mass, it is noted that the inclusion of such effects would have little effect on results at lower energies.[11]

While Tryon has raised the possibility that the $A_0^I(\nu)$ contain infinitely many complex zeros at infinity, he also claims that these functions can be approximated by dispersion relations at low energies.[12] A simplistic view of this problem would note that poles of F_I at $|\nu| = \infty$ would only affect the magnitudes of F_I in the low energy region; adjusting their magnitudes at the symmetry point to satisfy approximate crossing symmetry via subtraction constants thus removes the difficulty. For a more complete discussion see Ref. 12. The lack of poles of $A_0^I(\nu)$ on the nearby physical sheet associated with the absence of complex zeros in the analytic continuation of $F_I(\nu)$ above the real axis has already been noted.

The determination of parameters through derivative conditions from approximate crossing symmetry introduces errors caused by the truncation of partial wave series in the derivation of Eqs. (12) - (16). While waves higher than p were neglected in writing Eqs. (12) - (14), the effects of higher waves upon the second

and third derivative conditions were minimized by including parametrized threshold fits which were then removed by combining equations. It is possible to show a posteriori that the d and f-waves are small, even with respect to the small s-waves associated with small values of $|\lambda|$ (recall $A_0^0(sp) = -5\lambda$). The equations which were combined to remove the effects of those waves in deriving Eqs. (15) and (16) have been used to calculate their values at the symmetry point from the s and p-wave solutions presented in Section III C.[13] Even though the s-wave amplitudes vanish with λ, for each isospin state the magnitude of the d-wave amplitude is less than 4% of the magnitude of the s-wave amplitude for all of the solutions of Fig. 10, and this decreases to 1% for solutions with larger values of $|\lambda|$. More important, however, is how this affects the value of A_0^2 as calculated from $\lambda = -\frac{1}{5} A_0^0$ (evaluation at the symmetry point is implied throughout this discussion). When d and f-waves are included in Eq. (12) the value of A_0^2 is changed by

$$\Delta\left(A_0^2\right) = -\left(A_2^0 - \frac{5}{2}\, A_2^2\right) \quad . \tag{28}$$

The change for each of the solutions of Fig. 10 is listed in Table I, and in no case exceeds 2%.

For each of the solutions of Fig. 10 the f-wave amplitude is less than $\frac{1}{2}$% of the p-wave amplitude (at the symmetry point). Although it does not affect Eq. (28), it does affect the derivitive conditions for the s-waves, which also involve the slopes of the d-waves. For each isospin state, the slope of the d-wave amplitude ranges from $2\frac{1}{2}$% to 1% of the slope of the s-wave amplitude (at the symmetry point) for the solutions of Fig. 10. When d and f-waves are

included in Eqs. (13) and (14) the symmetry point slopes of the s-waves are changed by

$$\Delta\left(\frac{dA_0^0}{d\nu}\right) = \frac{63}{2} A_3^1 + \frac{5}{2} \frac{dA_2^0}{d\nu} \tag{29}$$

and

$$\Delta\left(\frac{dA_0^2}{d\nu}\right) = -\frac{63}{4} A_3^1 + \frac{5}{2} \frac{dA_2^2}{d\nu} \quad . \tag{30}$$

[The large factor multiplying the f-wave contirbutions in these equations is misleading - - note the p-wave multiplier in Eqs. (13) and (14).] These changes are also listed in Table I for the solutions of Fig. 10. The contributions to Eq. (30) tend to cancel yielding a maximum change of 2% for the I=2 s-wave slope, while the contributions to Eq. (29) tend to add. The percent change of the I=0 s-wave slope decreases from $7\frac{1}{2}$% for the solutions with $\lambda = -.033$ to $3\frac{1}{2}$% for the solution with $\lambda = .040$.

Although higher partial waves have been removed in the derivations of Eqs. (15) and (16) the restricted nature of the parametrization may also introduce errors. For instance, while in deriving Eq. (16) the f-wave is written as

$$A_3^1(\nu) = c\nu^3 \tag{31}$$

one may ask how the satisfaction of Eq. (16) would be affected if the f-wave were given by

$$A_3^1(\nu)' = a\nu^3 + b\nu^4 \tag{32}$$

with the same magnitude at the symmetry point and $a/b = 3$. When Eq. (16) is rederived keeping f-waves in general, and then the form of Eq. (32) is substituted in with parameters evaluated in terms of the calculated value of A_3^1

at the symmetry point the result is

$$\text{LHS} = \text{RHS} + \delta \tag{33}$$

where

$$\delta = \frac{675}{4} A_3^1 \tag{34}$$

The results calculated from the solutions of Fig. 10 are presented in Table II where the p-wave side of Eq. (16) is seen to be shifted by about 10%. If $a/b = -3$ the δ has the opposite sign and is about half as large.

While it should be possible to remove the errors in the magnitudes and slopes of the s-waves by incorporating d-wave effects into Eqs. (12) - (14) in an iterative manner, refinement of the second and third derivative conditions will require better knowledge of the d and f-waves, perhaps through iterated dispersion relations utilizing present s and p-wave solutions in the calculation of left cut integrals. The success of the present formalism in achieving sensible solutions makes it desirable to pursue such calculations. Consequently the possible effects of f-wave behavior on solutions selected by the third derivative condition are now discussed. As seen in Eqs. (33) and (34) the effect of unanticipated structure in the f-wave is to introduce a correction to the right hand (p-wave) side of Eq. (16) which is proportional to the symmetry point value of the f-wave amplitude. Inspection of Table II yields the fact that the correction is essentially a constant percentage of the p-wave side of Eq. (16). The effect of including such a correction in the formalism may be seen by shifting the p-wave curves of Fig. 9 appropriately, then identifying the solutions of Figs. 4, 5 and 6 which correspond to the λ values for which the curves of Fig. 9 intersect. Roughly, a 10% lowering of the p-wave curves of Fig. 9 (corresponding to the ratio $a/b=3$)

results in a 10% decrease in the mass of the predicted σ resonance for $|\lambda| < .02$. A 30% lowering (a/b=1.4) causes 20% decrease in σ masses. A 10% raising of the p-wave curves (a/b=-1.7) results in a 10% increase in the σ masses for $|\lambda| < .02$.

From the uncertainties documented above it is clear that an accurate application of derivative crossing conditions requires considerable care. This, of course, accounts for the popularity of the crossing conditions of Martin[14] which are less sensitive to truncation of the partial wave series. It is therefore of some interest to compare the solutions presented here with the results of independent calculations, also based on inverse amplitude dispersion relations, which use the Martin conditions in evaluating parameters.[15] In those calculations the s-waves were represented by functions similar to the $F_I(\nu)$ of this paper. The six s-wave parameters were fixed by matching the $F_I(\nu)^{-1}$ below threshold to solutions for $A_0^I(\nu)$ obtained from quadratic polynomial approximations to the amplitudes. The assumption that the Adler condition holds on the mass shell caused zeros of the s-wave amplitudes to coincide in all cases with those of the solution for $\lambda = -.008$ presented here. The solutions of Ref. 15 are ordered by a free parameter X; constraining X to positive values caused the polynomial amplitudes to satisfy eight conditions placed on the $\pi^0\pi^0$ scattering amplitudes. Solutions with $.7 \leq X \leq .5$ were preferred on the basis of agreement with experiment; the solution with $X = .7$ is in good agreement with the solution here presented for $\lambda = -.008$. Since the s-waves of both solutions are similarly parametrized and have sub-threshold zeros at coincident points one might expect that the crossing conditions used in Ref. 15 were satisfied by the $\lambda = -.008$ solution. Of the eight conditions,[16] only the sixth and seventh were unsatified, by 20 and 10 percent respectively. All conditions were satisfied by the solution with $\lambda = -.020$, while the solutions with $\lambda = .007$ was less satisfactory. One may speculate that

a more careful treatment of higher waves might induce changes in the solutions presented here which were somehow related to the lack of satisfaction of the Martin conditions. If so, the greatest changes would be expected in solutions with $\lambda > 0$, perhaps even yielding non-resonant solutions for realistically small values of λ. The significance of this possibility lies in the existance of such solutions in the literature.[7] While it is impossible to prove uniqueness in an iterated calculation, it seems reasonable that differences in the behavior of various solutions near the ρ mass may be mainly due to differences in the details of application of approximate conditions near and below threshold.

In summary, the solutions presented in Fig. 10 are known to contain errors due to approximations made in the derivation of derivative conditions from crossing symmetry which are used in the evaluation of s-wave parameters. However, solutions with $\lambda \lesssim -.01$ satisfy a set of crossing conditions derived so as to be insensitive to higher partial waves, and the solutions with $\lambda = -.008$ is in good agreement with independent results obtained without using derivative conditions. Thus the solutions with lower mass σ resonances may change little under improvement of the formalism. The imposition of derivative conditions to third degree from crossing symmetry is seen to provide a formalism which produces s-wave solutions above threshold with a sensible behavior as a function of λ, which also indicate a connection to earlier non-resonant solutions. In addition zeros of both s-wave amplitudes are found. The positions of the zeros are linearly related, and one solution has zeros which coincide with those obtained when the (off mass shell) Adler condition for PCAC is assumed to hold on the mass shell. The zeros appear naturally from the imposition of the crossing conditions, in the absence of any input from PCAC - - in fact the only input to the calculation is

the requirement that the p-wave exhibit a resonance of mass 755 MeV and width 120 MeV, which is used to fix the p-wave subtraction constants.

In order to improve the accuracy of the predictions of this model the following future modifications are proposed. First, the d and f-wave modifications to the zeroth and first derivative equations indicated in Eqs. (29) - (31) should be incorporated in the determination of parameters in an iterative way. Second, more accurate estimates of the d and f-waves at the symmetry point should be obtained using dispersion relations incorporating the s and p-wave results. These results should then be incorporated into the application of all derivative conditions used in the determination of s-wave parameters in an iterative way. Efforts are being initiated towards the accomplishment of these objectives.

V. ACKNOWLEDGMENT

It is a pleasure to acknowledge many discussions with Claude Kacser. The author is grateful to the National Science Foundation's Research Participation Program for College Teachers for the opportunity to carry out this investigation. The hospitality of the faculty and staff of the Center for Theoretical Physics, and of the Computer Science Center of the University of Maryland is also greatly appreciated.

FOOTNOTES

1. S. Weinberg, Phys. Rev. Letters 17 , 616 (1966).
2. G. F. Chew, S. Mandelstam and H. P. Noyes, Phys. Rev. 119 , 478 (1960).
3. B. H. Bransden and J. W. Moffat, Nuovo Cimento 21 , 505 (1961), Phys. Rev. Letters 8, 145 (1962), Nuovo Cimento 32 , 159 (1964).
4. K. Kang, Phys. Rev. 134 , B1324 (1964).
5. B. F. Gore, Phys. Rev. 183 , 1431 (1969).
6. G. F. Chew and S. Mandelstam, UCRL Report 9126 (Lawrence Radiation Laboratory, March 1960).
7. E. P. Tryon, Proceedings of the Conference on $\pi\pi$ and $K\pi$ Interactions, Argonne National Laboratory (May, 1969); Phys. Rev. Letters 20 , 769 (1968).
8. In evaluating the numerical integrals the integration variable was changed to $(\nu+1)^{-1/2}$ for $\nu > 0$ and $(-\nu)^{-1/2}$ for $\nu < -1$, and the unit interval of integration was divided into forty equal sub-intervals for evaluation by Simpson's rule. This grid, extremely fine near threshold and growing coarser with increasing $|\nu|$ allows a more accurate evaluation of the better known contributions near threshold. It was convenient to impose conditions at grid points, and the grid point closest to the ρ mass was at 745 MeV.
9. D. Morgan and G. Shaw, Nucl. Phys. B10 , 261 (1969); Phys. Rev. 10 , July (1970).
10. R. Bizzari, et al., Nucl. Phys. B14, 169 (1969).
11. Right cut effects occuring for $\nu > \nu_1$ only affect the left cut integrand through Eq. (7) for $\nu < -(\nu_1 + 1)$. Since the left cut integral is subtracted, the

effects of distant variations in its integrand are minimized. This arguement, plus the fact that by all estimates d-waves are thought to be small below (at least) the ρ mass, justifies the truncation of the integrand of Eq. (7) after p-waves.

12. E. P. Tryon, Columbia Univ. Reports NYO-1932(2)-188 and NYO-1932(2)-194.

13. d-waves were calculated using both the one parameter and two parameter d-wave threshold fits used to derive Eqs. (15) and (16). Results agreed within 10 to 20% for both magnitudes and slopes. Central values are used in the following discussion.

14. A. Martin, Nuovo Cimento 47 , 265 (1967); A. K. Common, ibid. 53A , 946 (1968).

15. J. B. Carrotte and R. C. Johnson, Phys. Rev. D2 , 1945 (1970).

16. Eqs. (20) to (27) of R. H. Graham and R. C. Johnson, Phys. Rev. 188 , 2362 (1969).

TABLE I

Symmetry point values of s-wave amplitudes and their derivatives for the solutions of Fig. 10 (method C). Also, the changes in these quantities computed a-posteriori due to inclusion of d and f-wave contributions (A_0^0 is related to λ, and hence does not change).

λ	A_0^0 / $-A_0^2$	$\Delta(A_0^2)$	$\frac{dA_0^0}{d\nu}$	$\Delta\left(\frac{dA_0^0}{d\nu}\right)$	$\frac{dA_0^2}{d\nu}$	$\Delta\left(\frac{dA_0^2}{d\nu}\right)$
-.033	.167	.0667	.0003	.200	-.015	-.1000	-.0036
-.020	.100	.0400	.0001	.196	-.013	-.0978	-.0036
-.008	.040	.0160	.0001	.191	-.011	-.0956	-.0036
.007	-.033	-.0133	-.0002	.184	-.010	-.0922	-.0023
.020	-.100	-.0400	-.0008	.177	-.008	-.0887	-.0003
.040	-.200	-.0800	-.0006	.169	-.006	-.0843	-.0025

TABLE II

Changes of the right hand (p-wave) side of Eq. (16) when the f-wave parametrization is changed,(a/b = 3) as discussed in the text.

λ	Eq. (16)	$10^4 A_3^1$	δ	%
.040	.008	.05	.0008	10
.020	-.025	-.11	-.0019	8
.007	-.061	-.34	-.0057	9
-.008	-.110	-.59	-.0100	9
-.020	-.147	-.86	-.0145	10
-.033	-.193	-1.1	-.0186	10

FIGURE CAPTIONS

1. s-wave phase shifts, labeled by λ, for typical solutions obtained when a σ of 745 MeV was required (method A).
2. s-wave scattering lengths, with λ values indicated, obtained when a σ of 745 MeV was required (method A).
3. Right and left hand sides of Eq. (16) as a function of λ for solutions obtained when a σ of 745 MeV was required (method A). The solid curve is the left (s-wave) side and the dashed curve is the right (p-wave) side.
4. Typical s-wave phase shifts for positive λ, obtained when $\delta_0^2 = -20^\circ$ at 745 MeV was required (method B). The solid curves show δ_0^0 and the dashed curves show δ_0^2. Since the δ_0^2 curves interpolate smoothly between bounding solutions, some have been left out for clarity. All phase shifts are modulo π.
5. Typical s-wave phase shifts, labeled by λ, obtained when $\delta_0^2 = -15^\circ$ at 745 MeV was required (method B). Solid and dashed curves are as in Fig. 4.
6. Typical s-wave phase shifts, labeled by λ, obtained when $\delta_0^2 = -10^\circ$ at 745 MeV was required (method B). Solid and dashed curves are as in Fig. 4.
7. Typical s-wave phase shifts for negative λ obtained when $\delta_0^2 = -20^\circ$ at 745 MeV was required (method B). Solid and dashed curves are as in Fig. 4.
8. s-wave scattering lengths of the solutions of Figs. 4-7 (method B). Values of δ_0^2 for solutions indicated by circles, triangles and squares are -20°, -15° and -10° respectively. The curves are from Ref. 2, a required σ of 900, 765 and 600 MeV yielding the upper, middle and lower curves respectively.
9. Right and left hand sides of Eq. (16) as a function of λ for solutions obtained when δ_0^2 was fixed at 745 MeV (method B).

10. Typical s-wave phase shifts, labeled by λ, obtained when Eq. (16) was imposed (method C).

11. The s-wave scattering lengths of the solutions of Fig. 10 (method C) are indicated by crosses, and labeled by λ values. Scattering lengths predicted by a linear extrapolation from the symmetry point of the s-wave amplitudes of these solutions are indicated by the vertical marks crossing the appropriately labeled dashed lines. These latter aspects of the figure are explained in the discussion after Eq. (30).

12. Zeros of the s-wave amplitudes of the solutions of Fig. 10 (method C) labeled by λ values. Weinberg's prediction is labeled PCAC and coincides with the solution for $\lambda = -.008$. The straight line is seen to pass through the points.

13. Imaginary parity of the s-wave amplitudes for $\nu < 0$. The solid curves are from crossing and the dashed curves are from the inverse amplitudes.

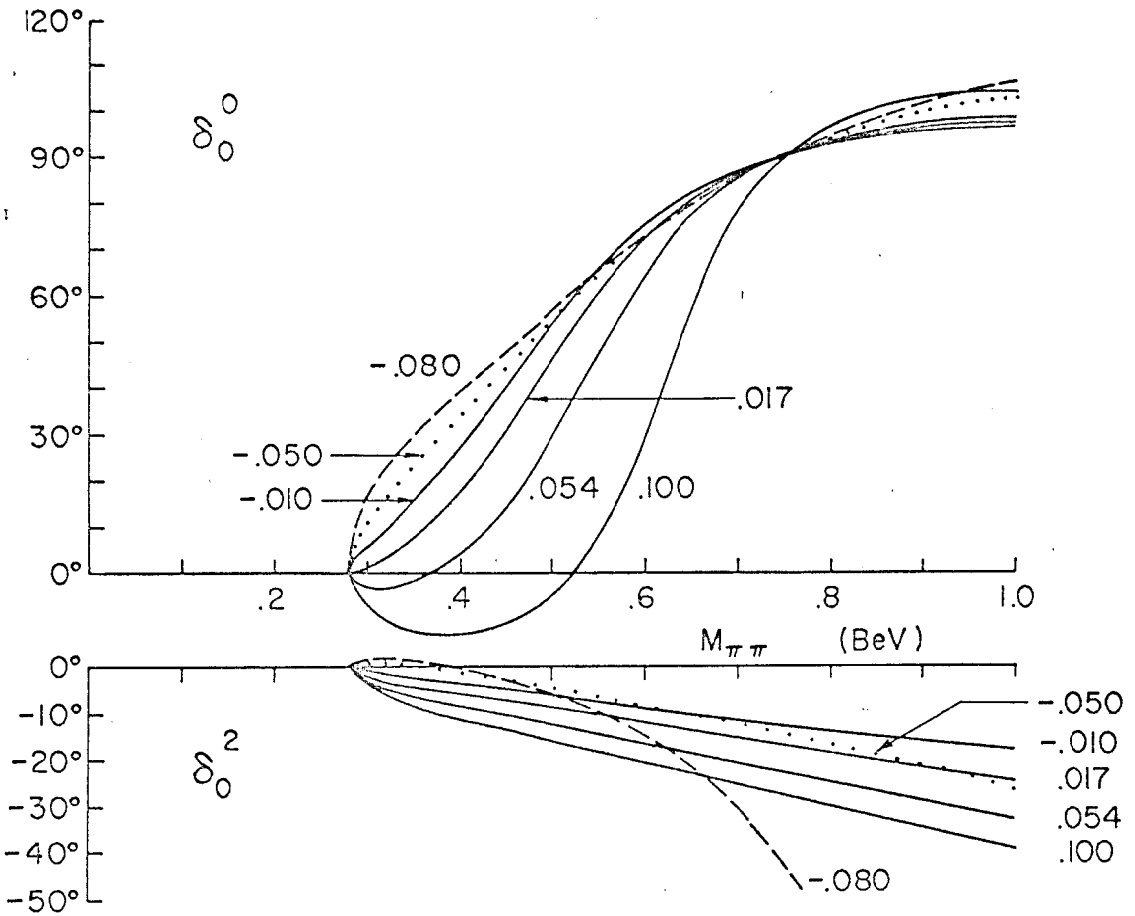
120°
90°
60°
30°
0°
δ_0^0
-.080
.017
-.050
-.010
.054
.100
.2
.4
.6
.8
1.0
$M_{\pi\pi}$ (BeV)
0°
-10°
-20°
-30°
-40°
-50°
δ_0^2
-.050
-.010
.017
.054
.100
-.080

Fig. 1

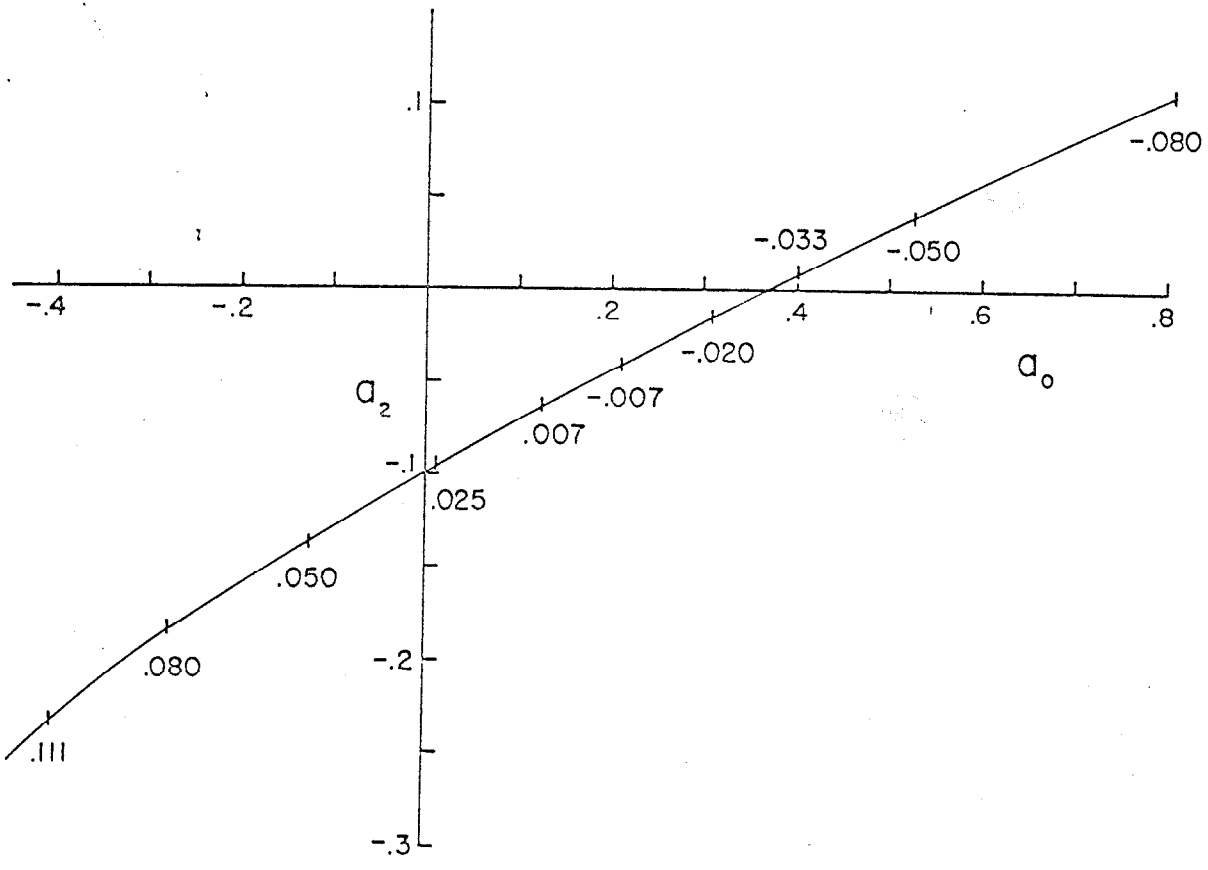

Fig. 2

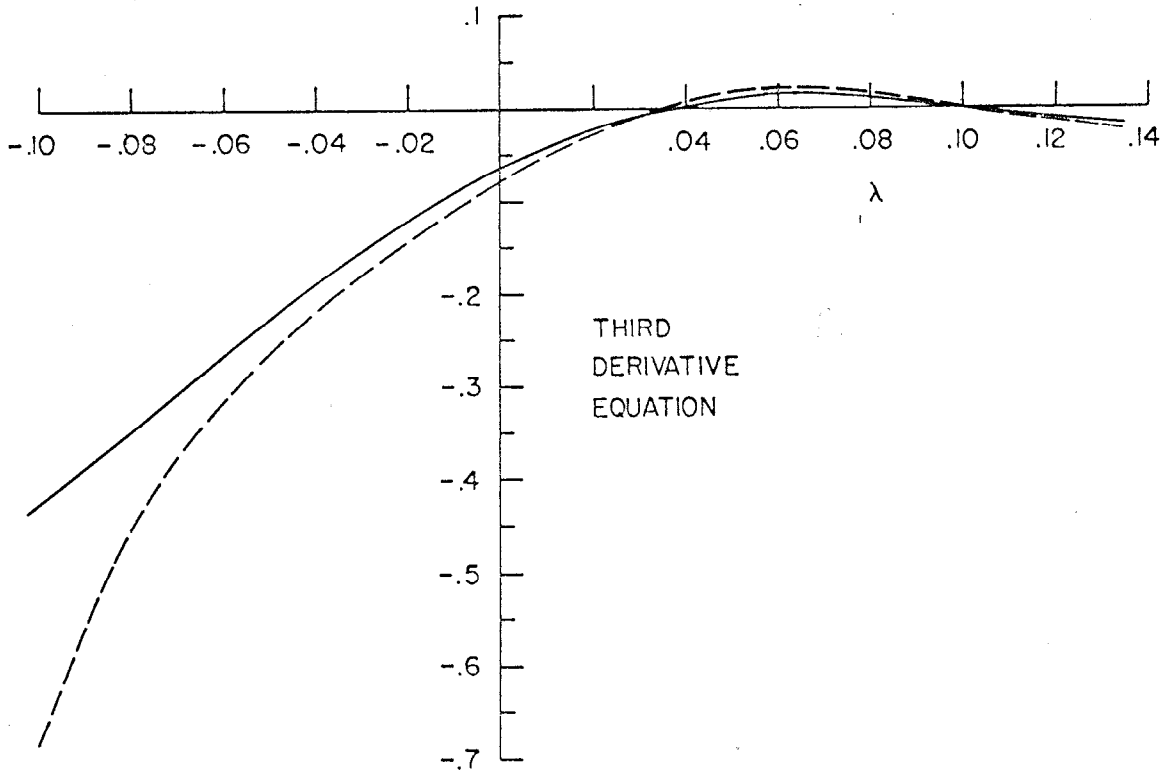
.1
-.10
-.08
-.06
-.04
-.02
.04
.06
.08
.10
.12
.14
λ
-.2
-.3
-.4
-.5
-.6
-.7
THIRD
DERIVATIVE
EQUATION

Fig. 3

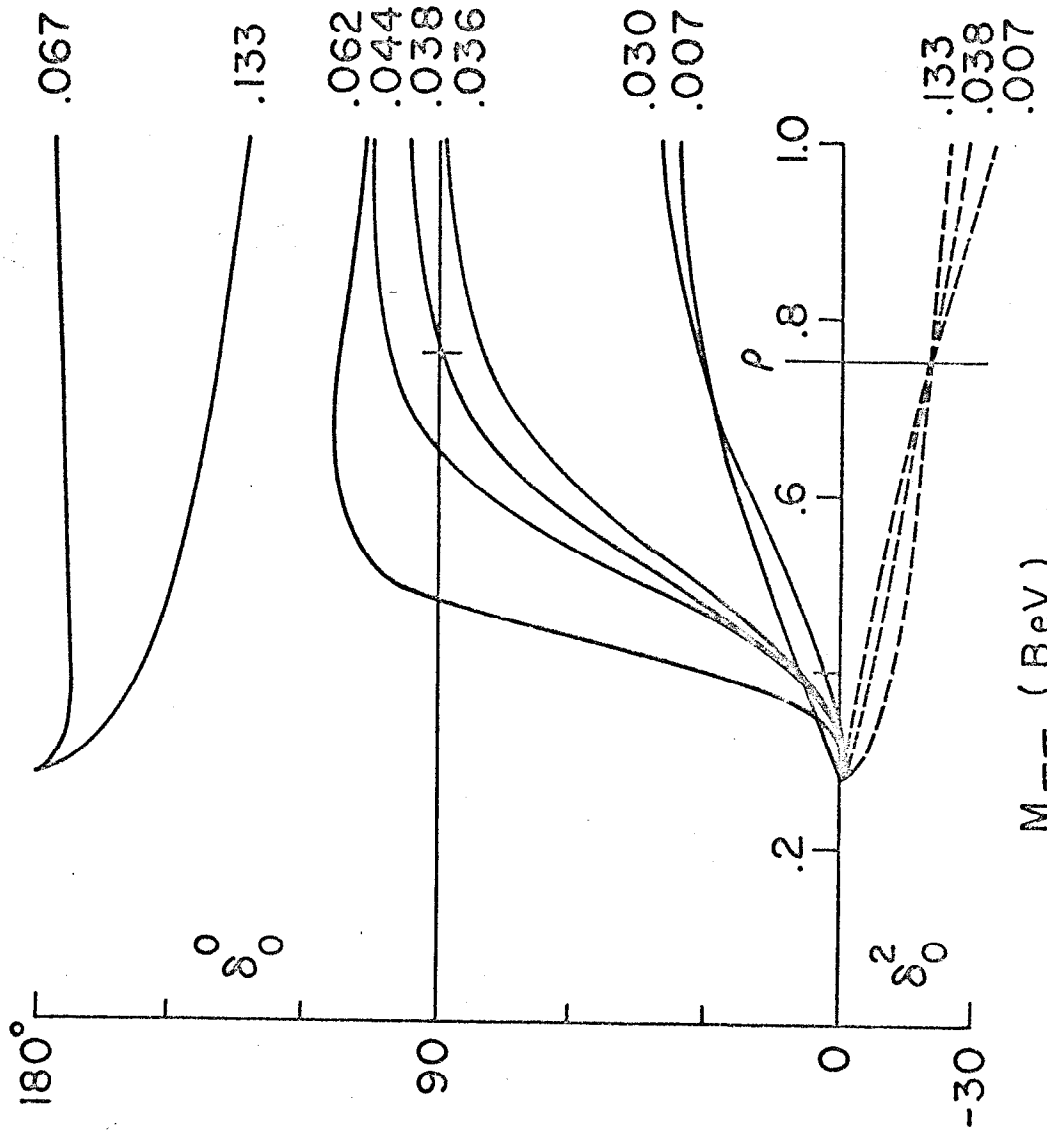
.067
.133
.062
.044
.038
.036
.030
.007
.133
.038
.007
180°
90
0
-30
δ_0^0
δ_0^2
.2
.6
.8
1.0
ρ
$M_{\pi\pi}$ (BeV)

Fig. 4

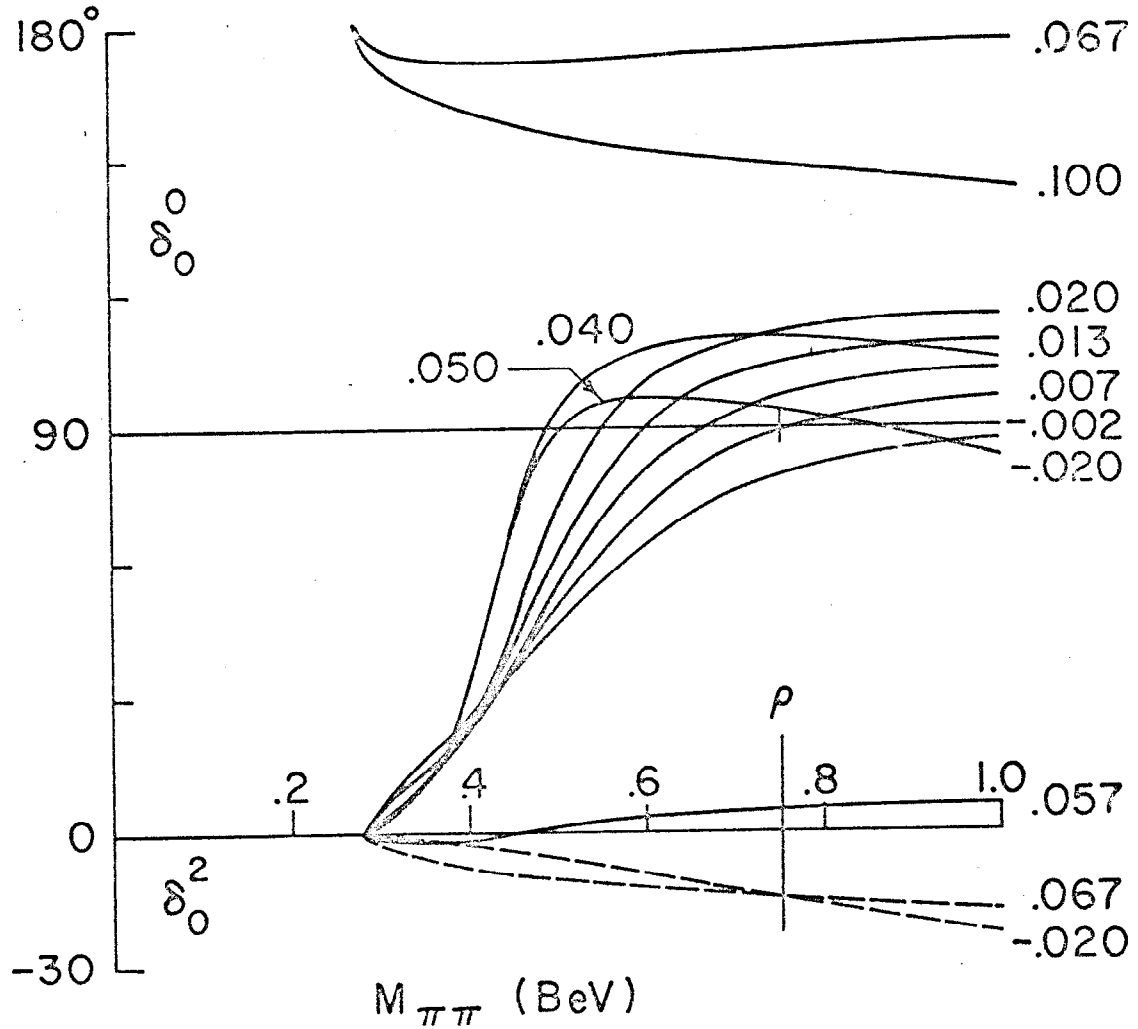
180°
90
0
-30
δ_0^0
δ_0^2
.067
.100
.020
.013
.007
-.002
-.020
.040
.050
ρ
.2
.4
.6
.8
1.0
.057
.067
-.020
$M_{\pi\pi}$ (BeV)

Fig. 5

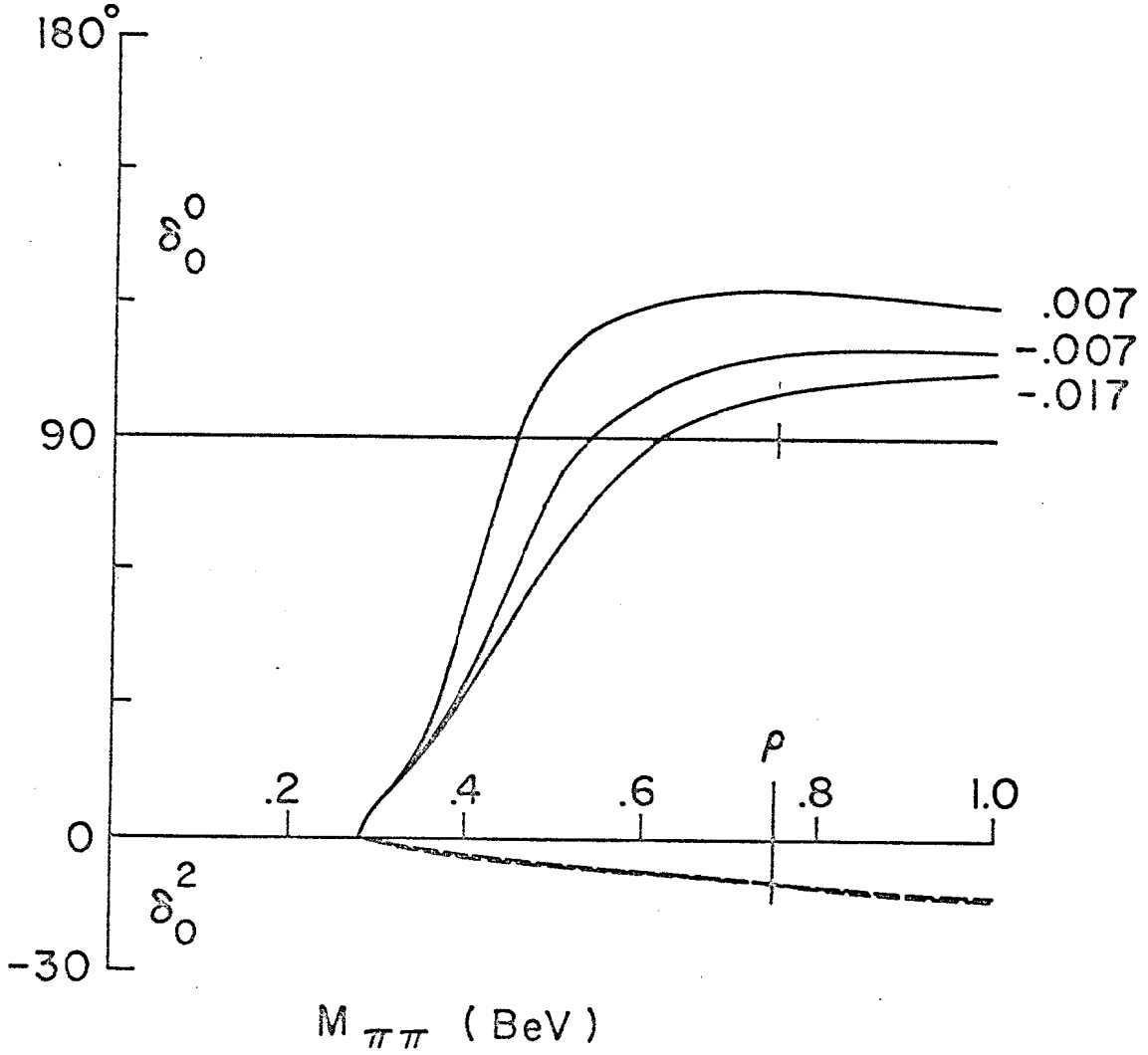

Fig. 6

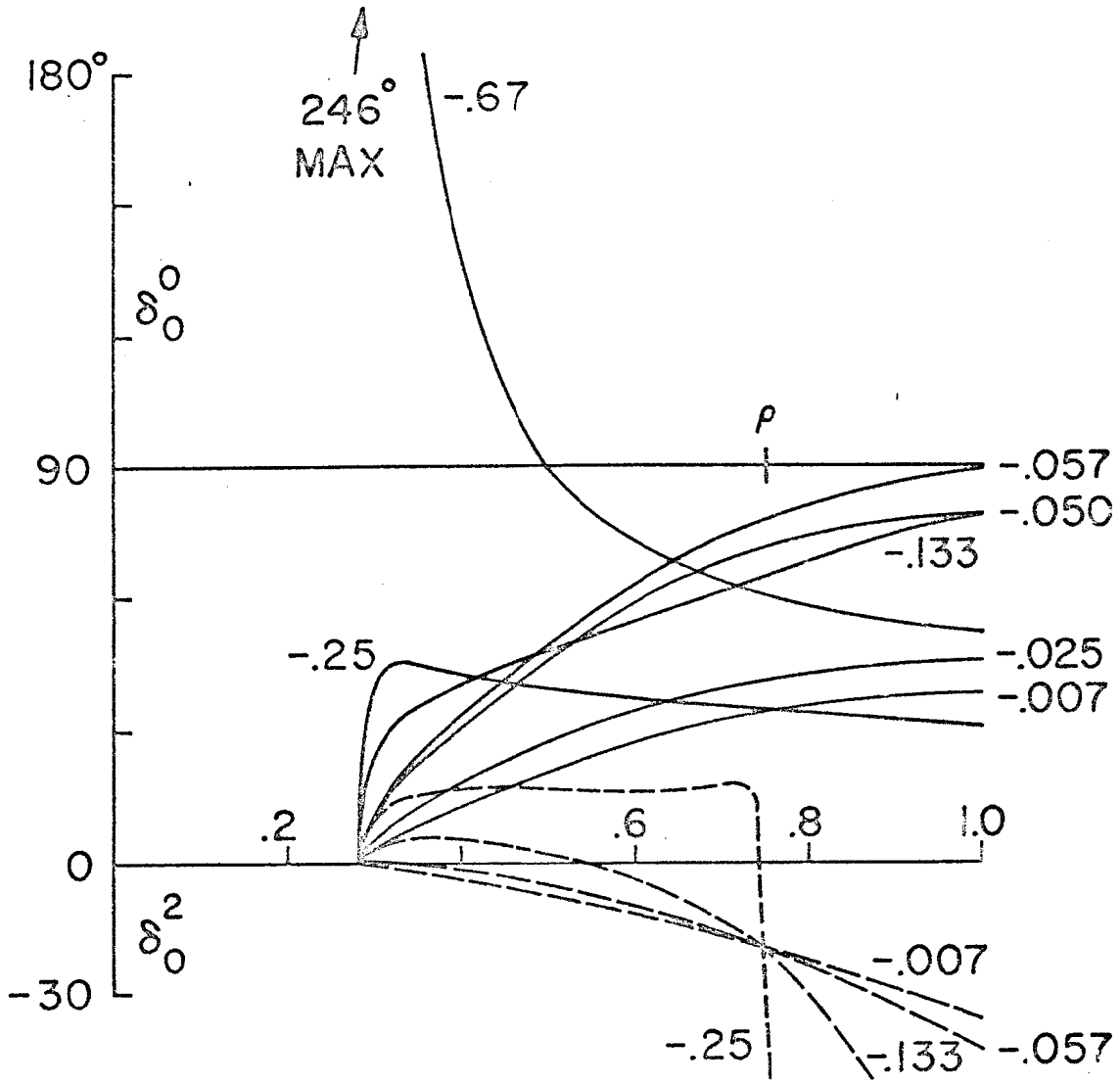
180°
246°
MAX
-.67
δ_0^0
ρ
90
-.057
-.050
-.133
-.25
-.025
-.007
.2
.6
.8
1.0
0
δ_0^2
-30
-.007
-.25
-.133
-.057
$M_{\pi\pi}$ (BeV)

Fig. 7

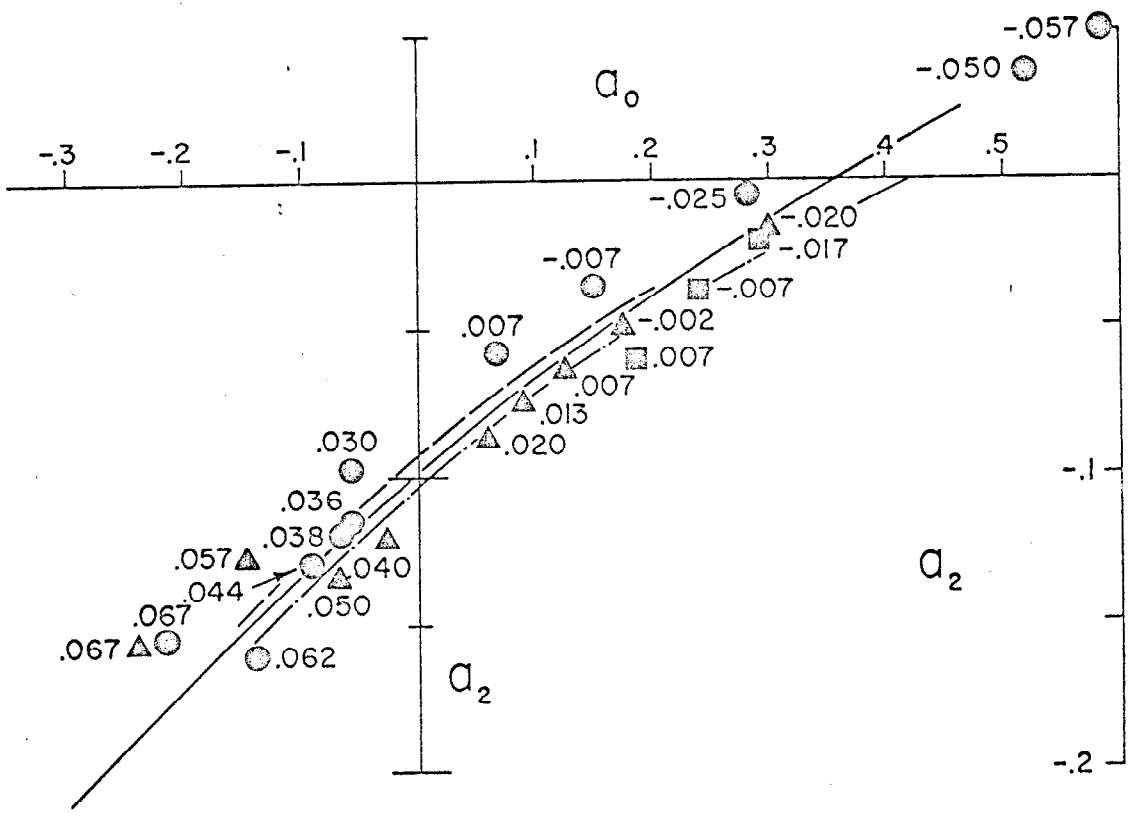
a_0
-.3
-.2
-.1
.1
.2
.3
.4
.5
-.057
-.050
-.025
-.020
-.017
-.007
-.007
-.002
.007
.007
.007
.013
.020
.030
.036
.038
.040
.044
.050
.057
.067
.067
.062
-.1
-.2
a_2
a_2

Fig. 8

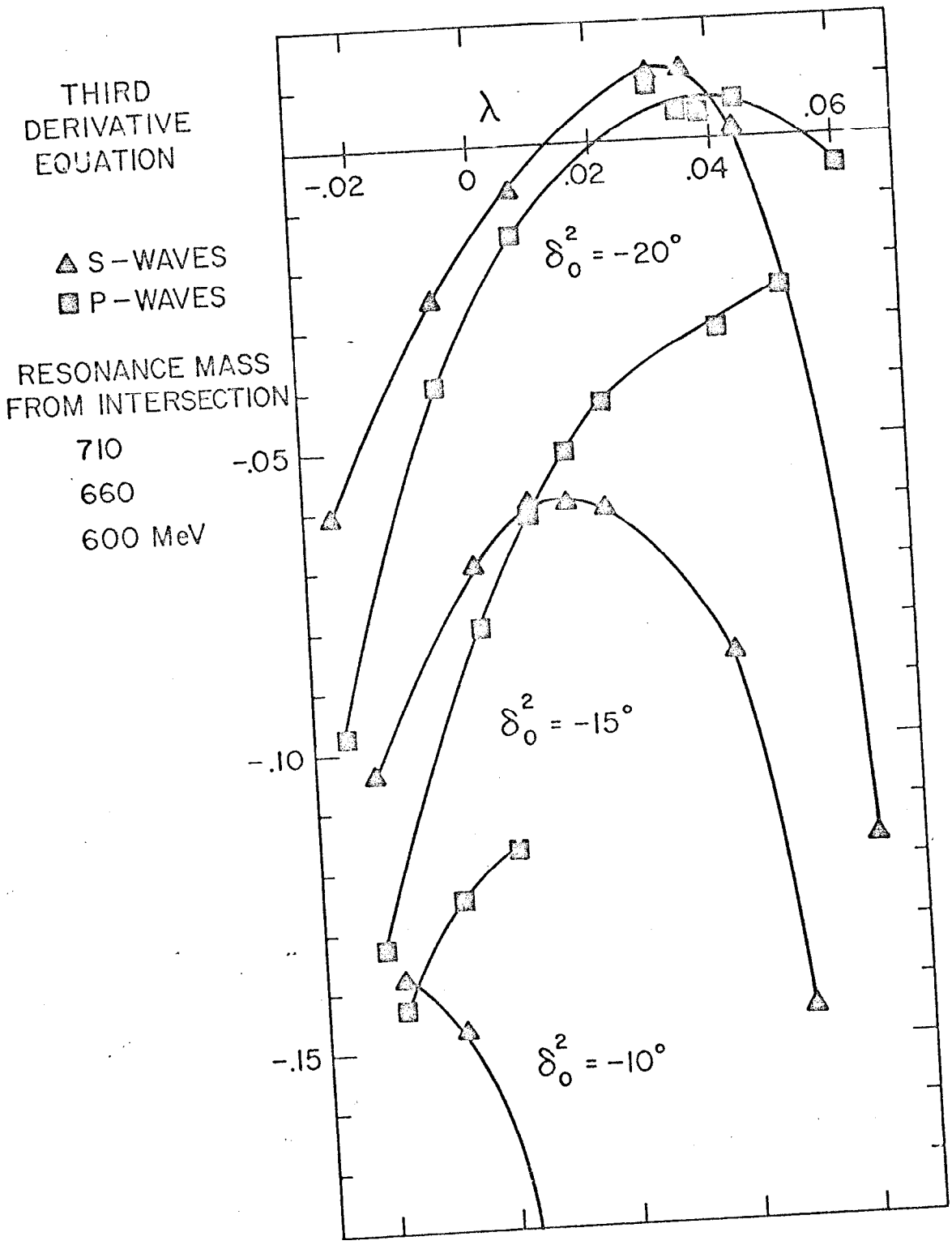
THIRD
DERIVATIVE
EQUATION
S-WAVES
P-WAVES
RESONANCE MASS
FROM INTERSECTION
710
660
600 MeV
λ
-.02
0
.02
.04
.06
-.05
-.10
-.15
$\delta_0^2 = -20°$
$\delta_0^2 = -15°$
$\delta_0^2 = -10°$

Fig. 9

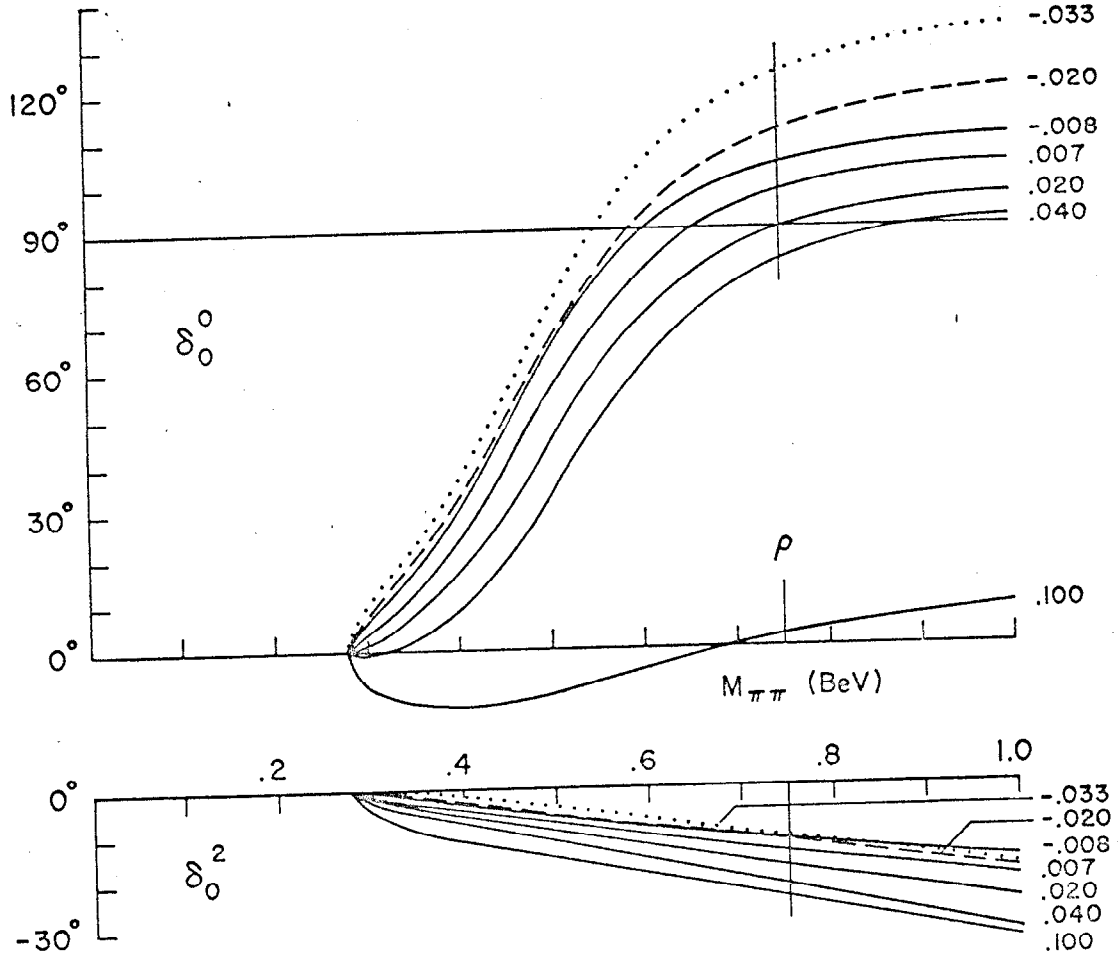
120°
90°
60°
30°
0°
δ_0^0
-.033
-.020
-.008
.007
.020
.040
ρ
.100
$M_{\pi\pi}$ (BeV)
.2
.4
.6
.8
1.0
0°
-30°
δ_0^2
-.033
-.020
-.006
.007
.020
.040
.100

Fig. 10

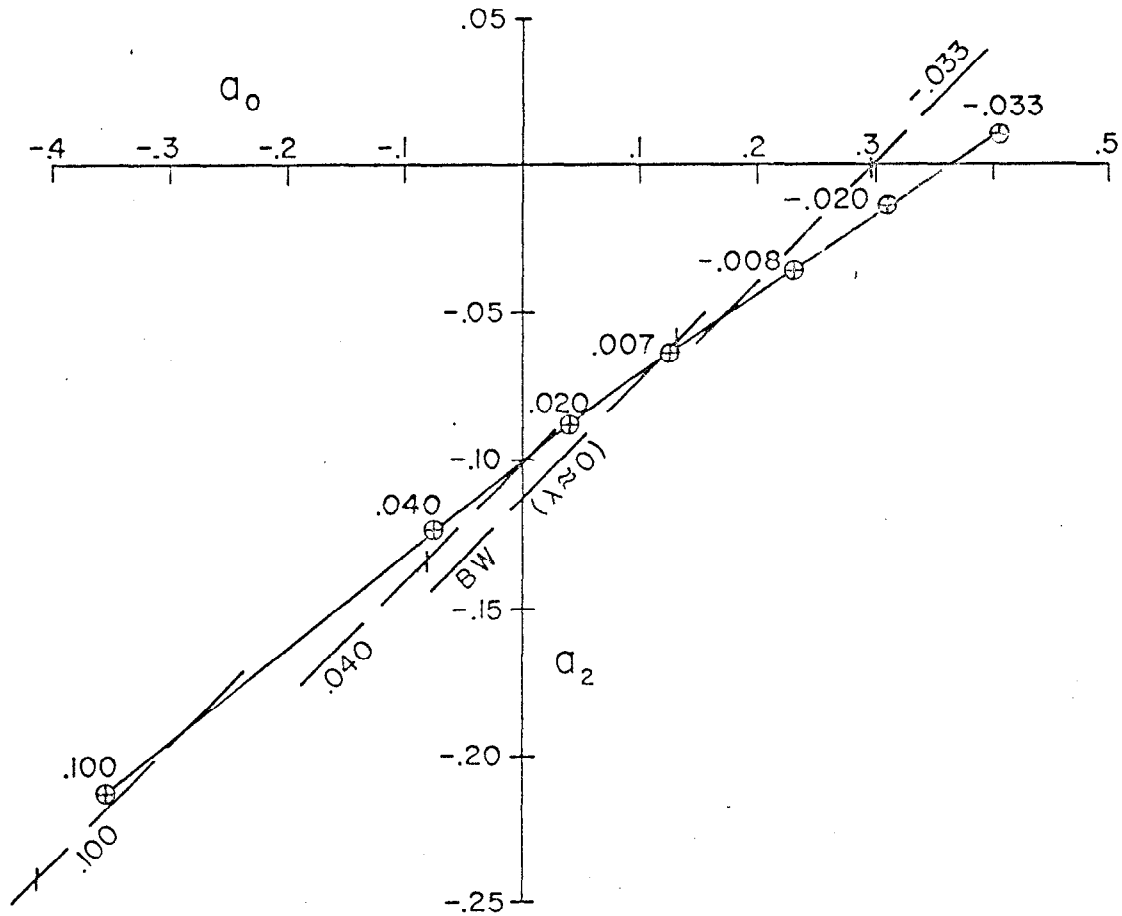
.05
a_0
-.4
-.3
-.2
-.1
.1
.2
.3
.5
-.033
-.033
-.020
-.008
-.05
.007
.020
-.10
.040
(0≤Y)
BW
-.15
a_2
.040
.100
.100
-.20
-.25

Fig. 11

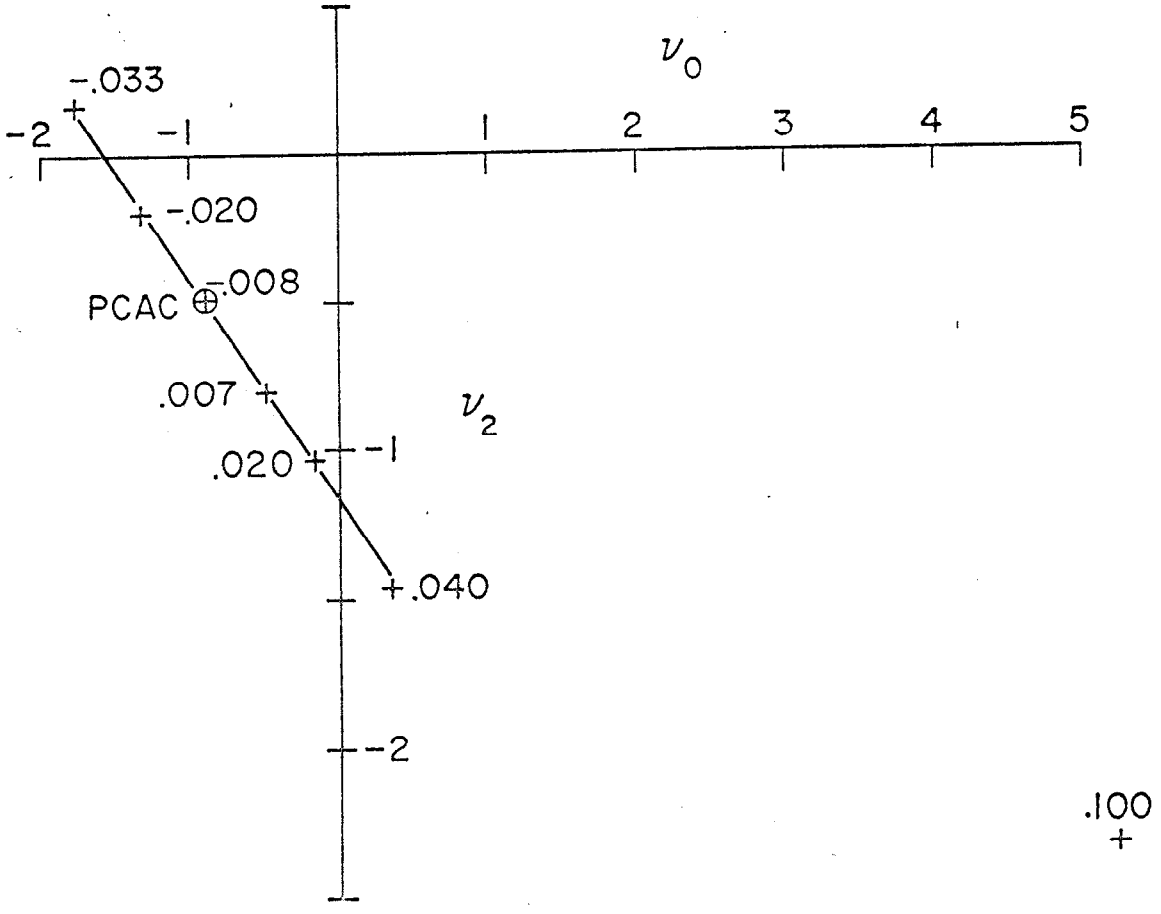

Fig. 12

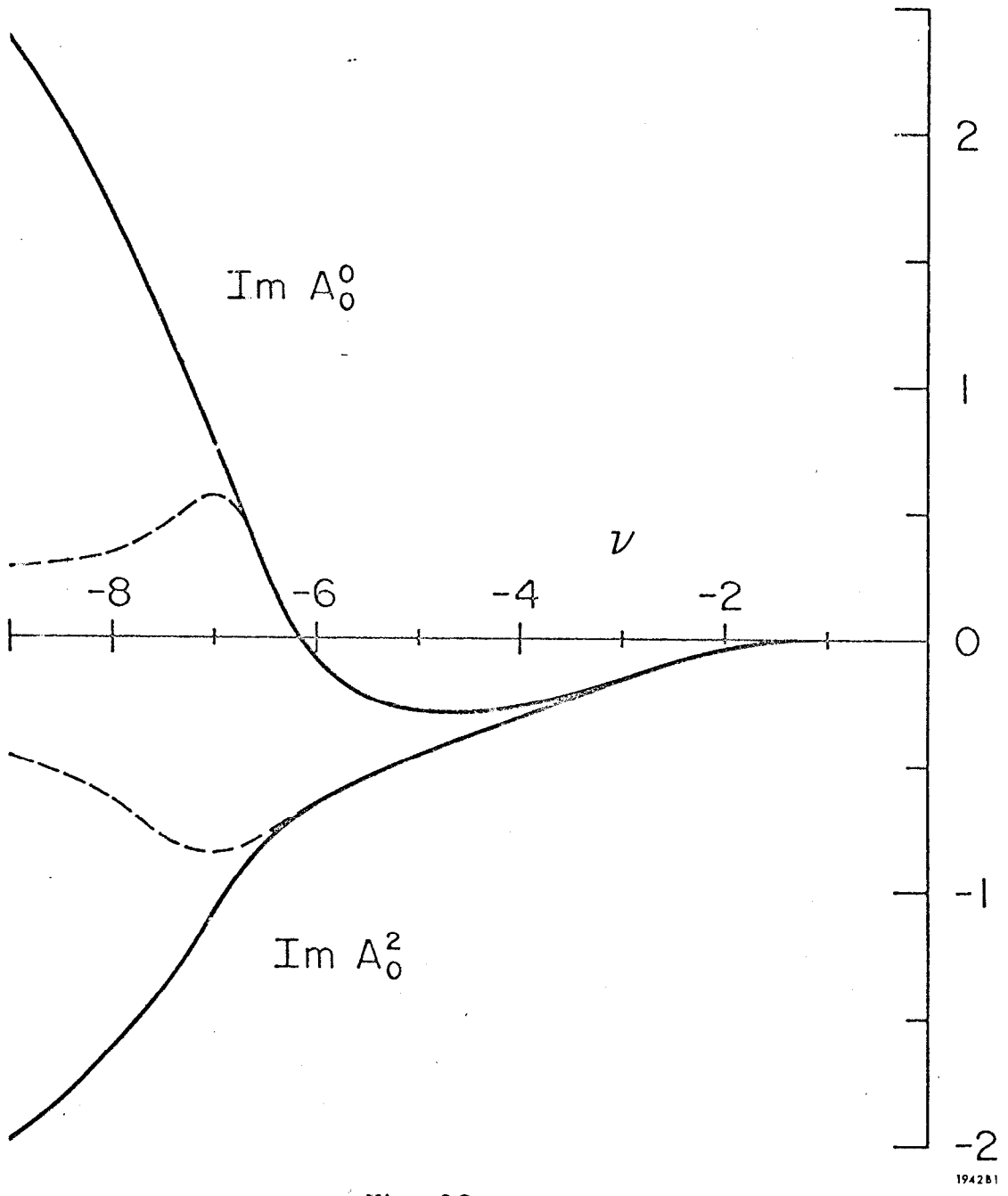

Fig. 13